Decoding continuous three-dimensional hand trajectories from epidural electrocorticographic signals in Japanese macaques

2012 J. Neural Eng. 9 036015

(http://iopscience.iop.org/1741-2552/9/3/036015)

J. Neural Eng. **9** (2012) 036015 (13pp) doi:10.1088/1741-2560/9/3/036015

Decoding continuous three-dimensional hand trajectories from epidural electrocorticographic signals in Japanese macaques

Kentaro Shimoda[1,2], **Yasuo Nagasaka**[1], **Zenas C Chao**[1] **and Naotaka Fujii**[1,3]

[1] Laboratory for Adaptive Intelligence BSI, RIKEN, 2-1 Hirosawa, Wako, Saitama 351-0198, Japan
[2] Department of Neurological Surgery, Nihon University School of Medicine, Tokyo 173-8610, Japan

E-mail: na@brain.riken.jp

Received 8 October 2011
Accepted for publication 3 May 2012
Published 25 May 2012
Online at stacks.iop.org/JNE/9/036015

Abstract
Brain–machine interface (BMI) technology captures brain signals to enable control of prosthetic or communication devices with the goal of assisting patients who have limited or no ability to perform voluntary movements. Decoding of inherent information in brain signals to interpret the user's intention is one of main approaches for developing BMI technology. Subdural electrocorticography (sECoG)-based decoding provides good accuracy, but surgical complications are one of the major concerns for this approach to be applied in BMIs. In contrast, epidural electrocorticography (eECoG) is less invasive, thus it is theoretically more suitable for long-term implementation, although it is unclear whether eECoG signals carry sufficient information for decoding natural movements. We successfully decoded continuous three-dimensional hand trajectories from eECoG signals in Japanese macaques. A steady quantity of information of continuous hand movements could be acquired from the decoding system for at least several months, and a decoding model could be used for ~10 days without significant degradation in accuracy or recalibration. The correlation coefficients between observed and predicted trajectories were lower than those for sECoG-based decoding experiments we previously reported, owing to a greater degree of chewing artifacts in eECoG-based decoding than is found in sECoG-based decoding. As one of the safest invasive recording methods available, eECoG provides an acceptable level of performance. With the ease of replacement and upgrades, eECoG systems could become the first-choice interface for real-life BMI applications.

1. Introduction

A major aspect of brain–machine interface (BMI) technology is the decoding of human intention from brain activity to generate commands for controlling motor neuroprosthetic devices [1]. The technology can help to substitute motor functions in individuals with an inability or restricted ability to perform voluntary movements, including patients suffering from amyotrophic lateral sclerosis, stroke, spinal cord injury or other neurological disorders [1–3]. Electrocorticography (ECoG) has been employed to record brain activity for BMI applications [4–6]. There are two types of ECoG: subdural ECoG (sECoG), which records electrical brain signals from beneath the dura, and epidural ECoG (eECoG), which records signals from above the dura. Compared with electroencephalography (EEG), which is the most commonly used non-invasive technique for recording brain activities, sECoG provides a much better signal-to-noise ratio, higher spatial resolution, and broader bandwidth with fewer artifacts [7]. Indeed, off-line decoding of sECoG signals has been used

[3] Author to whom any correspondence should be addressed.

to extract continuous three-dimensional (3D) hand motion information (hand kinematics) with much higher prediction accuracy than EEG-based decoding [EEG: 8, sECoG: 9]. For real-time BMI application, the training period required for sECoG-based BMI is much shorter than that required for EEG-based BMI (several hours versus several months) [EEG: 3, sECoG: 4, 5, 10]. Compared with single-unit activity (SUA), which is the most commonly used invasive technique for decoding, sECoG has comparable accuracy in predicting continuous arm motion with a high degree of freedom [SUA: 11–13, sECoG: 9], with the addition of three major advantages. (1) sECoG does not penetrate the brain parenchyma or cerebral blood vessels, suggesting that the risk of tissue damage and cerebral hemorrhage would be reduced. (2) sECoG can be used to extract signals from a wide range of cortical area, something that is not easy using SUA recordings. (3) The sECoG-based decoder provides long-term stability, offering stable performance for at least four months without recalibration [9], whereas SUA-based decoding requires recalibration at least daily [14]. Online sECoG-based BMI experiments in human subjects have shown one- and two-dimensional cursor control in epileptic patients [4, 5, 15] and the control of the three types of hand movements in poststroke patients [6].

Surgical complications are one of the main obstacles blocking clinical application of ECoG-based BMI technology. Complications in sECoG implementation, mostly caused by the direct pressure of the electrodes on the cerebral cortex, include subdural hematoma, intracerebral hemorrhage, cerebral infarction, cerebral edema, and permanent neurological deficits [16–20]. Moreover, epidural hematoma and infection could occur in both sECoG and eECoG implementations [21–25]. The incidence of complications in studies using sECoG or eECoG is shown in table 1. It is worth noting that direct comparisons among these studies might not be fair, since different studies might have different conditions, such as the number of electrodes implanted, the size of incision, and the duration of implantation, etc. Nonetheless, eECoG is theoretically safer than sECoG for long-term implementation for the following four reasons. (1) eECoG electrodes are unlikely to press the arachnoid membrane directly and interfere with arterial or venous circulation. (2) eECoG electrodes are unlikely to injure cortical arteries or bridging veins. (3) Even if infection developed around the electrodes in the epidural space, it would be unlikely to extend into the brain and cause more severe conditions than would occur with sECoG because the dura would act as a barrier [26]. Despite the size of the brain area contacted or pressed by the electrodes, infection in the epidural space carries less risk of permanent damage to the brain than infection in the subdural space. (4) The dura is not opened in eECoG implantation, which makes the operation shorter and consequently lowers the risk of infections [27]. Therefore, eECoG is thought to be safer than sECoG for long-term implementation.

In animal studies, simple motor outputs have been decoded using eECoG. In rats, an eECoG-based decoder was used to classify four types of body movements, achieving an accuracy of 73.2% [28], and the two-dimensional reach direction was decoded with an accuracy of 69% [29]. Additionally, four levels of grasp force were decoded from eECoG signals in monkeys, and the prediction accuracy was comparable to decoding of local field potentials [30]. In a poststroke hemiparetic patient, an eECoG decoder was used to discriminate arm movement within one degree of freedom (flexion and extension) with an accuracy of 90% [31]. Moreover, eECoG has been applied for more complex and real-time decoding as well as in studies decoding simple motor outputs. Online eECoG-based BMI experiments have demonstrated one- and two-dimensional cursor control in monkeys [32–35], and binary switch and one-dimensional cursor movement could be achieved by online eECoG-based BMI in human patients [36, 37]. However, decoding higher dimensional natural movements is helpful for the real-life application of realistic motor prosthetics, and it remains unclear whether eECoG signals can provide as much information for decoding continuous 3D hand trajectories as is possible in sECoG studies.

In the present study, we implanted eECoG array and successfully decoded 3D hand trajectories in Japanese macaques during an asynchronous food-reaching task, in which no explicit cues were provided to initiate movement. eECoG was found to have long-term durability, suggesting that it could become a practical interface for real-life BMI applications in the future.

2. Methods

2.1. Subjects and surgical procedure

Two adult Japanese macaques (monkeys B and C) were implanted with customized 64-channel ECoG electrodes (Unique Medical, Tokyo, Japan) in the epidural space of the left hemisphere covering the area from the prefrontal cortex (PFC) to the primary somatosensory cortex (S1) [38]. The locations of the electrodes were identified by overlaying magnetic resonance imaging scans and x-ray images (figure 1(a)). Platinum electrodes were 2.1 mm in diameter, with 1 mm diameter exposed from the silicone sheet. The inter-electrode distance was 3.5 mm. The reference electrode was a rectangular platinum plate (5 mm × 10 mm) placed in the epidural space, and the ground electrode was the same type of rectangular platinum plate placed above the skull, in contrast to our previous sECoG study, in which the reference electrode was placed in the subdural space and the ground electrode was placed in the epidural space [9]. The leads from the eECoG electrodes were soldered with connectors (Omnetics Connector Corporation, Minneapolis, MN, USA) and fixed to the skull with resin and titanium screws.

Monkey C was previously implanted with nodule-type electrodes in the subdural space of the primary motor cortex (M1) and the dorsal premotor cortex (PMd) for a different study (unpublished). Moderate granulation was observed beneath the dura when we removed the subdural nodule-type electrodes. Although there was possible damage in the M1 and PMd owing to the implantation, it was presumably only minor damage because we observed normal behavior without any sign of paralysis in monkey C.

Table 1. Complications in eECoG and sECoG implementation.

Type of electrodes	Reports	Number of patients (number of monitored sessions)	Duration of implementation (days)	Total complications	Hematoma	Infection	Cerebral infarction	Cerebral edema	Permanent neurological deficit	Other complications
eECoG	Tsubokawa 1993 [21]	11	>288	0 (0%)						
	Katayama 1998 [22]	31	>288	1 (3.2%)		1 (3.2%)				
	Levy 2008 [23]	12	42	1 (8.3%)						1 (8.3%)
	Nguyen 1999 [24]	32	1440	3 (9.4%)	1EDH (3.1%)	1 (3.1%)				1 (3.1%)
	Nguyen 2008 [25]	10	360	0 (0%)						
sECoG	Fountaus 2007 [16]	185	2-25	18 (9.7%)	3 EDH (1.6%) 2 SDH (1.1%)	2 (1.1%) 2 osteomyelitis (1.0%)		2 (1.1%)		9 (4.9%)
	Van Gompel 2008 [17]	189 (198)	2-24	26 (13.1%)	6 (30%)	2 empyema (1.0%) 1 abscess (0.5%)			3 (1.5%)	12 (6.1%)
	Wong 2009 [18]	71 (79)	7-14	26 (33%)	1 (1.3%)	2 ostemyelitis (2.5%)	1 (1.3%)	1 (1.3%)		21 (27%)
	Hamer 2002 [19]	187 (198)	1-34	*52 (26.3%)	5 EDH (2.5%) 3 EDH (1.6%)	18 (9.1%)			9 (4.5%)	20 (10.1%)
	Morrell 2011 [20]	191	364	*225 (117.8%)	4 SDH (2.1%) 2 ICH (1.0%)	10 (5.2%)				*206 (107.9%)

Abbreviations: EDH, epidural hematoma; SDH, subdural hematoma; ICH, intracerebral hemorrhage.
* Some patients suffered from multiple complications.

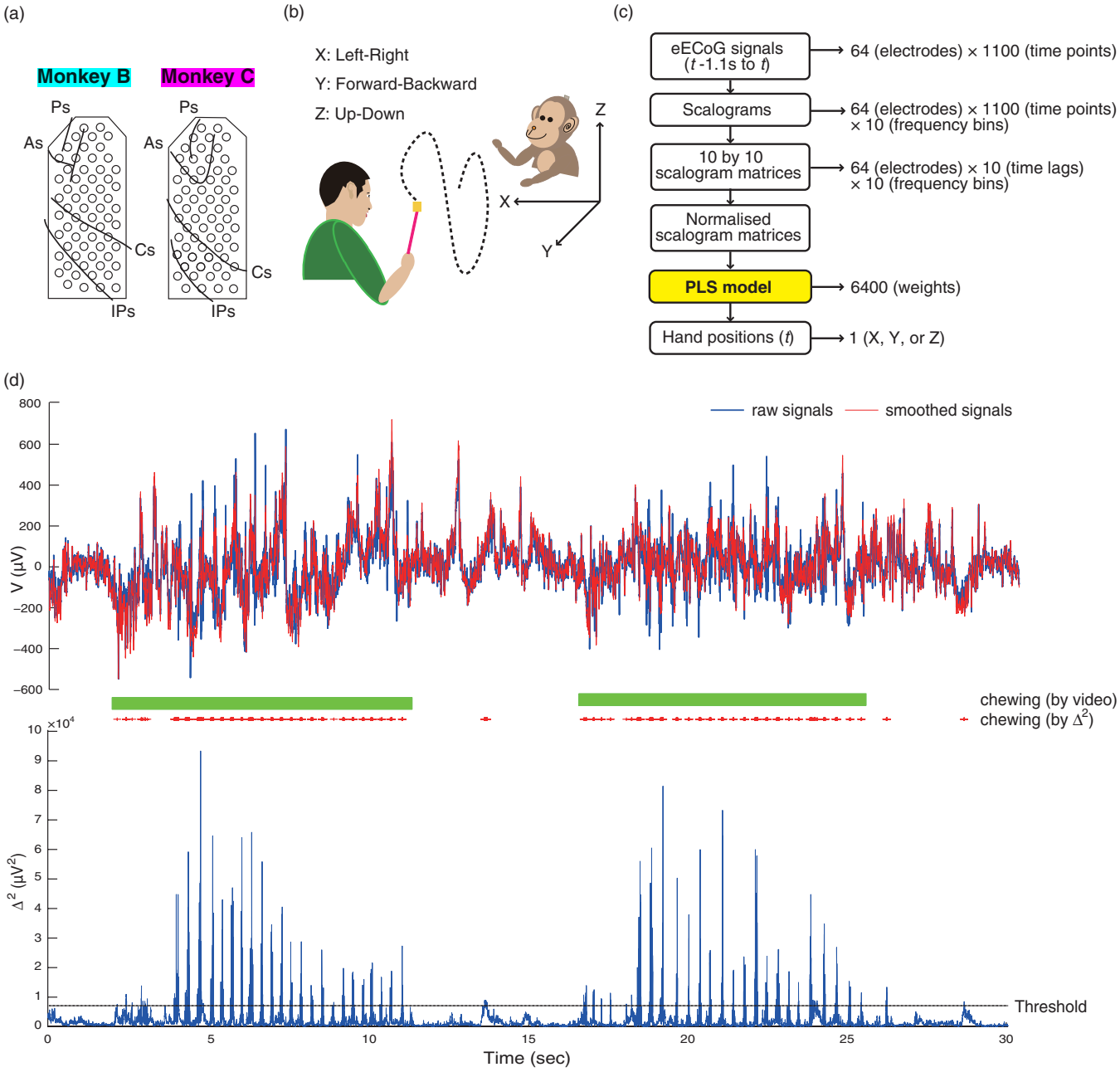

Figure 1. Experimental protocol, decoding scheme, and extraction of chewing artifacts. (a) Each monkey was implanted with 64 electrodes in the epidural space of the left hemisphere, covering the area from the prefrontal cortex to the parietal cortex. Ps: principal sulcus; As: arcuate sulcus; CS: central sulcus; IPs: intraparietal sulcus. (b) In the asynchronous food-reaching task, the monkey retrieved foods from random locations with random intervals. The body-centered coordinates used to measure hand positions in 3D space are shown. (c) Diagram showing each step for predicting hand positions at time t from eECoG signals and the dimensionality of each variable (see section 2.3). (d) Top: Representative raw (blue) and smoothed signals (red) from one channel in a 30 s window. Bottom: Δ^2 in the corresponding window (see section 2.5). Red + symbols indicate the time points where Δ^2 was over the threshold (dashed line). Green bars indicate the actual mastication periods identified in the video.

The methods used for skin incision, osteotomy, and fixation of the connector can be found at Neurotycho.org[4] [38].

2.2. *Experimental protocol*

Each monkey was trained to retrieve foods using the right hand, being contralateral to the implanted hemisphere (figure 1(b)). During each 15 min experiment, each monkey was fed foods by the experimenter at random locations using a fork length of 20 cm with random intervals (3.8 ± 1.0 times per minute, mean ± SD, $n = 20$ recording sessions, two monkeys). Each trial was started after the monkey finished chewing the food. For monkey B, 10 recording sessions were performed over 40 days following a postoperative period of five months. For monkey C, ten recording sessions were performed over two months following a postoperative period of three months.

[4] http://wiki.neurotycho.org/Surgical_Procedure

eECoG signals were recorded with a sampling rate of 1 kHz per channel, using two data acquisition systems: Cerebus (Blackrock Microsystems, Salt Lake City, UT, USA) for monkey B, and Digital Lynx (Neuralynx, Bozeman, MT, USA) for monkey C. Each monkey's hand motion was recorded by an optical motion capture system with a sampling rate of 120 Hz (Vicon Motion Systems, Oxford, UK). During the task, monkeys were seated in a custom-made chair facing the experimenter with head movement restricted. All procedures were performed in accordance with protocols approved by the RIKEN ethics committee. All of the data used in this paper are available at Neurotycho.org [38].

2.3. Decoding paradigm

We used a previously proposed paradigm for off-line decoding [9]. eECoG signals of 1 kHz were band-pass filtered from 0.3 to 500 Hz, and were re-referenced by common average referencing for data analyses. Briefly, we attempted to predict the instantaneous 3D hand position at time t from brain signals during the previous 1 s. 3D hand positions were calculated by referencing the wrist position of the reaching hand to body-centered coordinates (X: left–right, Y: forward–backward, Z: up–down, figure 1(b)). The time–frequency representation of brain signals at each electrode was described by a scalogram generated by Morlet wavelet transformation at ten different centre frequencies ranging from 10 to 120 Hz (figure 1(c)). The scalogram of time t was calculated from the eECoG signals from $t - 1.1$ s to t. The scalogram was then resampled at ten time lags ($t - 0.1$ s, $t - 0.2$ s, ..., to $t - 1.0$ s) to form a 10×10 scalogram matrix. The standard z-score at each frequency bin was calculated to form a 10×10 normalized scalogram matrix, in which the same scale was shared across frequencies. A normalized motor parameter at time t was modeled as a linear combination of 6400 variables (64 electrodes $\times$ 10 frequency bins $\times$ 10 time lags) measured prior to time t with a constant term, where the 6400 weights described the spatio-spectro-temporal information inherent in the eECoG signals (figure 1(c)). To estimate the 6400 weights that represented a decoding model, multivariate partial least-squares (PLS) regression was applied on the training data (first 10 min) using ten-fold cross-validation, in which the optimal number of PLS components was determined by the minimal predictive error sum of squares. Those PLS components represented the latent structure in the 6400 dimensional space. Data recorded during the last 5 min were used for validation, in which decoding performance was quantified based on the correlation coefficients between the predicted and observed hand trajectories.

2.4. Spatio-spectro-temporal contributions

To investigate how information inherent in brain activity is integrated to control arm motion, the contribution of the spatio-spectro-temporal contents of the decoding model was quantified. Three different contents were calculated from $\{a_{\mathrm{ch,freq,lag}}\}$, which is the weight for the scalogram component at electrode 'ch', frequency 'freq', and time lag 'lag' in each decoding model:

$$W_s(ch) = \frac{\sum_{\mathrm{freq}}\sum_{\mathrm{lag}} |a_{\mathrm{ch,freq,lag}}|}{\sum_{\mathrm{ch}}\sum_{\mathrm{freq}}\sum_{\mathrm{lag}} |a_{\mathrm{ch,freq,lag}}|};$$

$$W_f(\mathrm{freq}) = \frac{\sum_{\mathrm{ch}}\sum_{\mathrm{lag}} |a_{\mathrm{ch,freq,lag}}|}{\sum_{\mathrm{ch}}\sum_{\mathrm{freq}}\sum_{\mathrm{lag}} |a_{\mathrm{ch,freq,lag}}|};$$

$$W_t(\mathrm{lag}) = \frac{\sum_{\mathrm{ch}}\sum_{\mathrm{freq}} |a_{\mathrm{ch,freq,lag}}|}{\sum_{\mathrm{ch}}\sum_{\mathrm{freq}}\sum_{\mathrm{lag}} |a_{\mathrm{ch,freq,lag}}|}. \quad (1)$$

The spatial contribution (W_s(ch)) of each recording electrode 'ch' was quantified based on the ratio of the absolute value of weight for the frequency bin and the time lag in the recording electrode to the total weight of all frequency bins and time lags. The spectral contribution (W_f(freq)) of each frequency bin 'freq' was quantified based on the ratio of the absolute value of weight for the recording electrode and the time lag in the frequency bin to the total weight of all recording electrodes and time lags. The temporal contribution (W_t(lag)) of each time lag 'lag' was quantified based on the ratio of the absolute value of weight for the recording electrode and the frequency bin in the time lag to the total weight of all recording electrodes and frequency bins.

2.5. Extraction of chewing artifacts

Artifacts in eECoG signals were observed during mastication. Sharp peaks with large amplitudes were found in signals during chewing periods and identified as chewing artifacts (upper panel in figure 1(d)). To identify these, raw signals were first smoothed by convolution of the Chebyshev window (window length = 10 samples, stop-band = 10 dB). Then, the square of the difference between the raw and smoothed signals was calculated for each time point and averaged across channels. A representative time course of this mean squared difference, or Δ^2, during both chewing and non-chewing periods, is shown in the lower panel in figure 1(d). Chewing periods were identified on the basis of a threshold, calculated by adding two standard deviations to the amplitude of the averaged Δ^2 at all time points during the recording session. The timings of chewing artifacts identified using this threshold were confirmed by video (green bar in figure 1(d)).

3. Results

3.1. Performance of eECoG-based decoding

To quantify the performance of eECoG-based decoding, correlation coefficients (r) between observed and predicted trajectories were calculated. The average correlation coefficients were 0.47 $\pm$ 0.12, 0.56 $\pm$ 0.1 and 0.68 $\pm$ 0.06 (mean $\pm$ SD, $n = 20$ recording sessions, two monkeys) for the X-, Y-, and Z-positions, respectively (figure 2). A representative 5 min record of the predicted hand positions in 3D space is

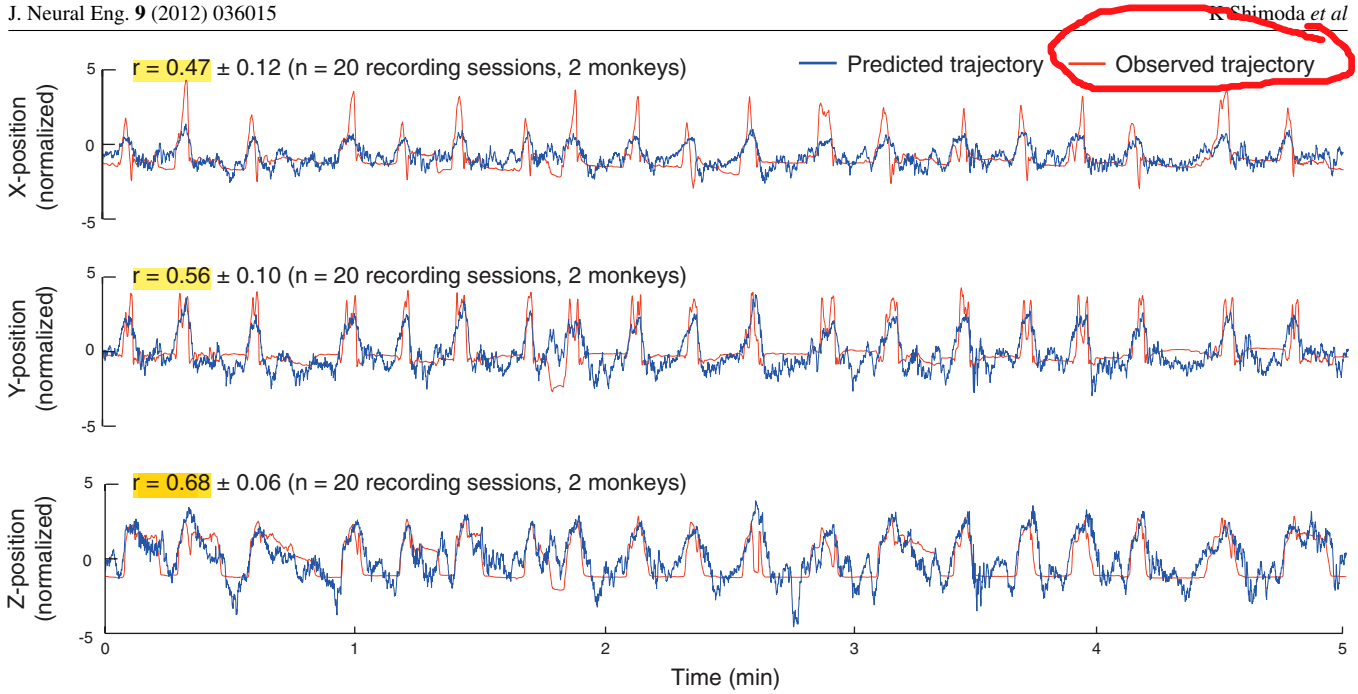

Figure 2. Representative asynchronous 3D hand trajectory decoding in a 5 min validation session. The average correlation coefficients between the predicted (blue) and observed (red) trajectories for *X*-, *Y*- and *Z*-positions are shown.

shown in figure 2. For both monkeys, the average correlation coefficient was highest for the *Z*-position and lowest for the *X*-position.

The optimal number of PLS components for decoding models was 36.3 ± 14.0 ($n = 20$ recording sessions, two monkeys). This number was significantly lower than the total number of variables included (6400 for monkeys B and C). This indicates that a small portion of the information carried in eECoG signals, representing the latent structure independent of the original data's dimensionality, was sufficient for obtaining an accurate prediction.

3.2. Long-term durability and stability

The durability of the recording system and the stability of the decoding model are important factors for implementing practical neuroprosthetics. To evaluate the durability of the eECoG-based system, the 3D hand positions were predicted using the decoding model constructed based on training data obtained immediately before the validation data (same-day prediction). The prediction accuracy of eECoG-based decoding showed no significant monotonic decrease for at least 1.5 months in monkey B, and for at least 2 months in monkey C ($p = 0.16$ for monkey B and 0.41 for monkey C, Spearman rank correlation test, $n = 10$ recording sessions for each monkey) (figure 3(a)). This result indicates that eECoG has long-term durability and that signal quality is maintained for several months at least. Moreover, the experiments were started a couple of months after implantation (five months after implantation for monkey B, three months for monkey C), which suggests that the durability of eECoG-based decoding could be longer than the recording period.

Calibration of the decoding model is usually needed in BMI applications to maintain prediction accuracy; therefore, an application with minimal need for calibration would result in more convenient BMI. To evaluate the stability of our eECoG-based decoding system, the decoding model constructed from each experiment was used to predict the validation data from subsequent experiments (cross-day prediction). To determine whether a decoding model could maintain a robust performance over a long period of time, the accuracies of every ten cross-day predictions with the closest durations were compared with the accuracies of ten same-day predictions, and the *p*-values were plotted against the mean durations of every ten cross-day predictions (figure 3(b)). There was no significant difference between the accuracies of cross-day prediction and same-day prediction for nine days in monkey B ($p > 0.01$ for *X*-, *Y*-, and *Z*-positions, Wilcoxon rank-sum test) and 20 days in monkey C (20 days for *X*-position, 40 days for *Y*-position, and 25 days for *Z*-position) (figure 3(b)). Our results indicate that the eECoG-based decoding model can be used on data collected weeks after construction of the model with no sacrifice of prediction accuracy.

3.3. Spatio-spectro-temporal contributions

Examining the weights in decoding models could further reveal neural information representing hand motion. The model can be simplified by using only the extracted neural information. Such a model would reduce the amount of calculation required and leads to more efficient BMI. Thus, the contributions of different domains (i.e. electrode locations, frequency bandwidths, and time lags) were evaluated. For monkey B, the spatial contributions were significantly greater than their medians in the PMd for *X*-, *Y*-, and *Z*-positions ($p < 0.01$, $n = 10$ recording sessions, Wilcoxon signed-rank test, thick circles in figure 4(a)). For monkey C, significant

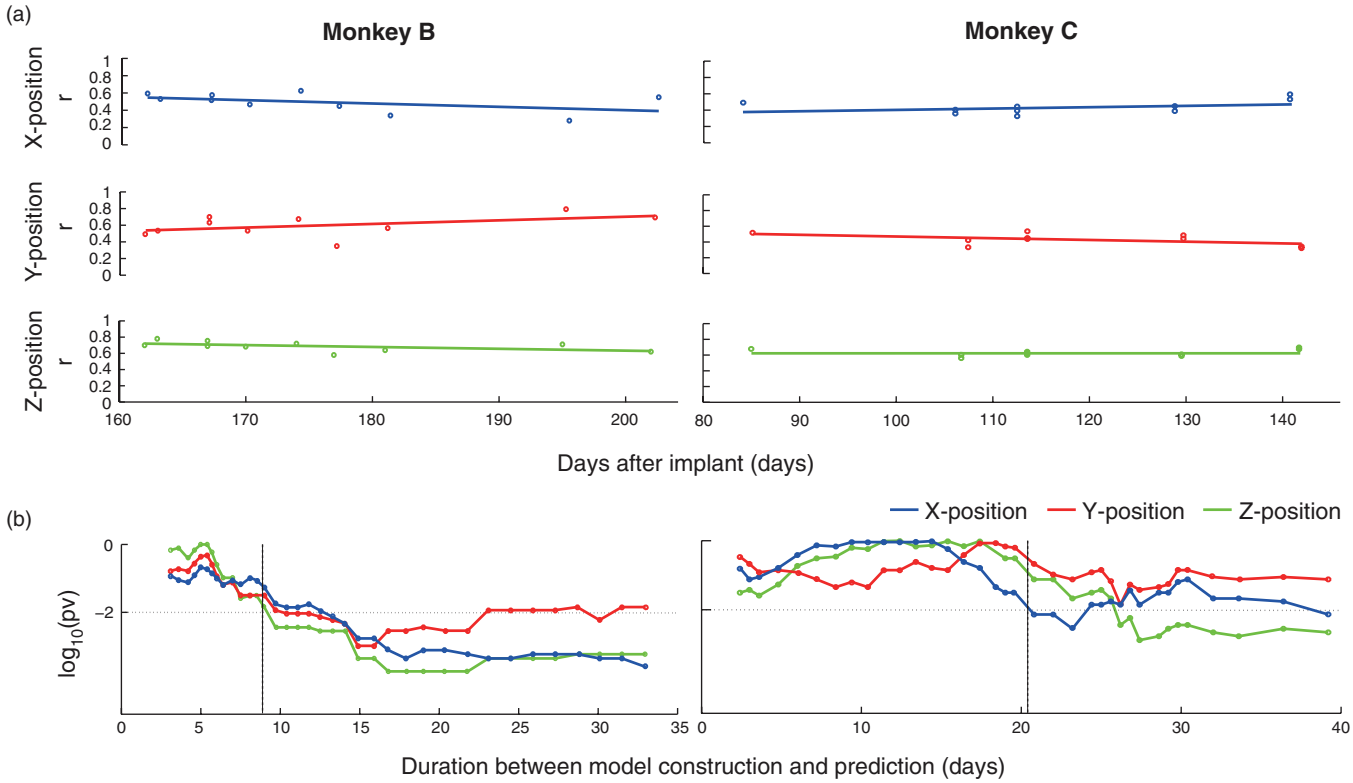

Figure 3. Long-term durability and stability of the decoding system. (a) Same-day prediction. The *x*-axis shows the duration from electrode implantation to the recording sessions. Correlation coefficients (r) are shown with fitted 1-degree polynomials (lines) for *X*-, *Y*-, and *Z*-positions ($n = 10$ recording sessions for each monkey). The recording system showed durability for at least 1.5 months and 2 months for monkeys B and C, respectively, with no significant monotonic decrease in prediction accuracy ($p = 0.16$ for monkey B, and 0.41 for monkey C, Spearman rank correlation test). (b) Cross-day prediction. *P*-values (pv, in the logarithmic scale) for comparisons of every ten consecutive cross-day data points with ten same-day predictions are shown. The threshold of 0.01, or -2 in the logarithm base 10 scale, is shown as horizontal dashed lines. The vertical dotted line indicates the earliest day on which the pv for at least one position dropped below the threshold (9 days and 20 days for monkeys B and C, respectively). Each decoding model could be used for nine days with steady performance.

spatial contributions were found in the PFC and S1 for all positions, and in the M1 for *Y*- and *Z*-positions ($p < 0.01$, $n = 10$ recording sessions, thick circles in figure 4(a)). For monkey B, the spectral contributions were significantly greater than their medians, between 40 and 70 Hz for the *X*-position, between 50 and 90 Hz for the *Y*-position, and between 40 and 90 Hz for the *Z*-position ($p < 0.01$, $n = 10$ recording sessions, asterisks in figure 4(b)). For monkey C, significant spectral contributions were found between 10 and 30 Hz for all positions ($p < 0.01$, $n = 10$ recording sessions, asterisks in figure 4(b)). Temporal contributions were significantly greater than their medians within the 500 ms before the predicted instant for both monkeys ($p < 0.01$, $n = 10$ recording sessions for each monkey, asterisks in figure 5(c)).

3.4. Chewing noise in eECoG signals

To determine the cause of the lower prediction accuracy in eECoG-based decoding compared with sECoG-based decoding, chewing artifacts were investigated to see how much contamination could be found in eECoG signals. Artifacts were successfully identified using the algorithm described in section 2.5. Examples of eECoG signals during mastication are shown in figure 5(a). Examples of sECoG signals from a previous report are also shown (figure 5(a), lower traces) to provide a contrast [9]. Chewing artifacts were rhythmical and synchronized with mastication. The artifacts had higher amplitudes than signals outside the chewing period. To quantify the degree of contamination from the chewing artifacts in recorded signals, the chewing artifacts index, defined as the ratio of the mean squared amplitude of signals within the chewing period to the mean squared amplitude of signals outside the chewing period, was calculated for each recording session. The chewing artifacts index of eECoG signals was significantly greater than that of sECoG signals ($p < 0.05$; for eECoG, $n = 20$ recording sessions, two monkeys; for sECoG, $n = 13$ recording sessions, two monkeys; Kruskal–Wallis test) (figure 5(b)). One of the two monkeys in the present study was different from the monkeys used in our previous report, but the electrodes used to obtain sECoG data were of the same type and the same cortical areas were recorded from [9]. The significantly higher chewing artifacts index in eECoG signals indicates that the eECoG system is more susceptible to contamination from chewing artifacts than the sECoG system.

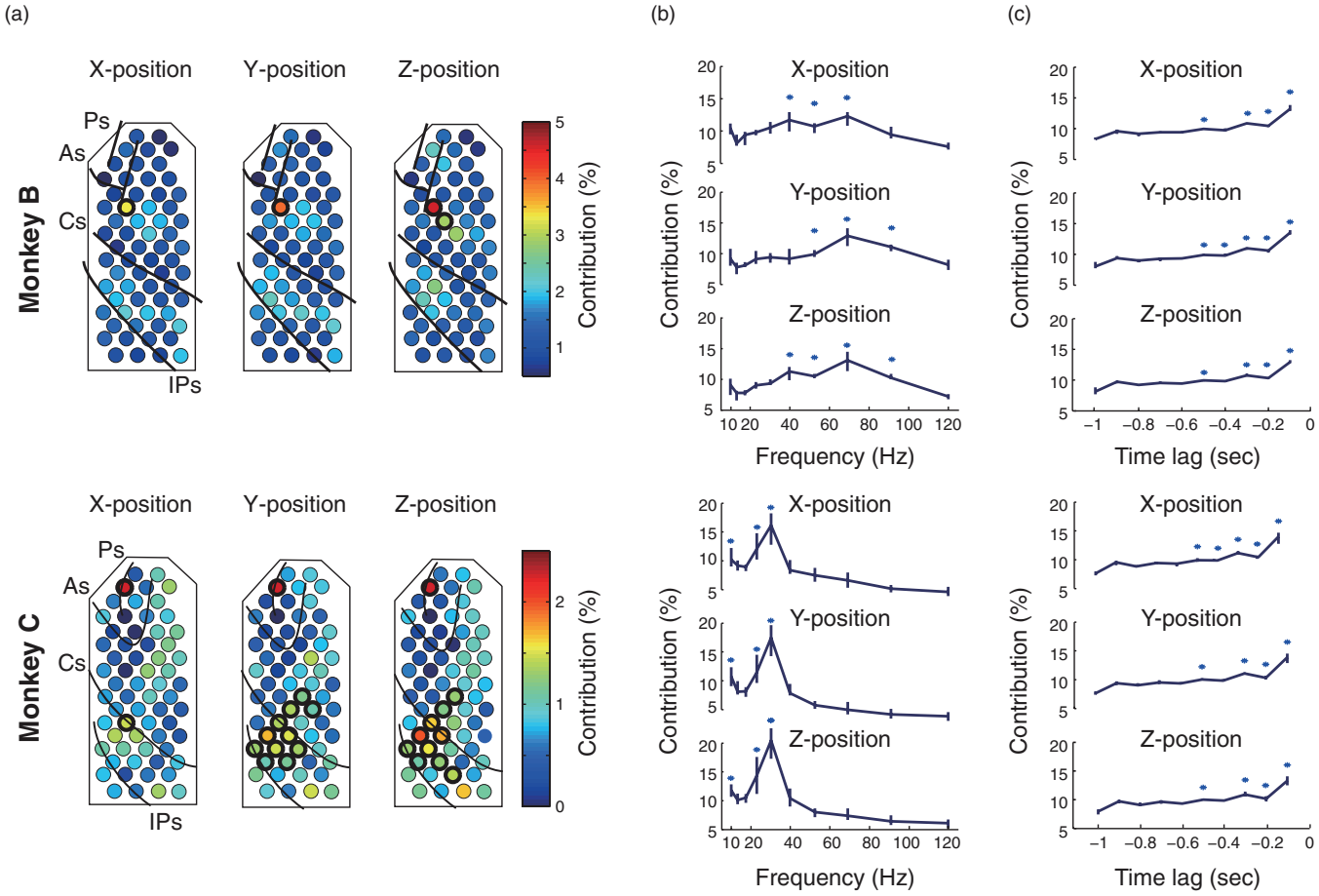

Figure 4. Spatio-spectro-temporal contributions in decoding models. (a) Spatial contributions at different electrodes. For each hand position, electrodes with contributions significantly greater than their median ($p < 0.01$, $n = 10$ recording sessions, Wilcoxon signed-rank test) are circled by thicker lines. Significant spatial contributions were found in the PMd for monkey B, and in the PFC, S1, and M1 for monkey C. (b) Spectral contributions in different frequency bins. For each hand position, the frequency bins with contributions significantly greater than their median ($p < 0.01$) are marked with asterisks. Significant spectral information ranged from 40 to 90 Hz (high-γ band) for monkey B, and from 10 to 30 Hz (β band) for monkey C. (c) Temporal contributions of different time lags. For each hand position, the time lags with contributions significantly greater than their median ($p < 0.01$) are marked with asterisks. Significant temporal information was found within 500 ms before the predicted instant for both monkeys.

3.5. Effect of noise level on decoding performance

To determine whether the chewing artifacts affected decoding performance, the relationships between decoding accuracies (correlation coefficients) and the chewing artifacts indices for eECoG ($n = 60$ correlation coefficients from 20 recording sessions) and sECoG ($n = 39$ correlation coefficients from 13 recording sessions, the same data set as in section 3.4) data were plotted (figure 6(a)). As shown in figure 6, there was a significant monotonic decrease in prediction accuracy with increasing chewing artifacts index ($p < 0.05$, $\varrho = -0.39$, Spearman rank correlation test). This indicates that the chewing artifacts index has a significant effect on decoding performance. Comparing sECoG and eECoG datasets, the chewing artifacts index was higher in eECoG datasets than in sECoG datasets, and the distribution of chewing artifacts index was wider (figure 6(b)), suggesting that the chewing artifacts index from eECoG data is less stable over time than that from sECoG data (figure 3(b)).

4. Discussion

4.1. Prediction accuracies in eECoG- and sECoG-based decoding

The present findings suggest that eECoG-based decoding methods can predict asynchronous 3D hand trajectories, reflecting more natural and intuitive movements than those examined in previous eECoG studies [28–37]. However, the accuracy of eECoG-based decoding was lower than that of sECoG-based decoding. Compared with our previous study using sECoG-based decoding, the mean correlation coefficients obtained using eECoG-based decoding were lower by 33.8%, 23.9% and 9.3% for *X*-, *Y*- and *Z*-positions, respectively [9]. To explain the difference in prediction performance between eECoG and sECoG, we focused on the *quality* and *quantity* of motor information inherent in the ECoG signals.

Importantly, we found the chewing artifacts index was higher in eECoG signals than in sECoG signals (figure 5(b)). As shown in figure 6(a), there was a significant negative

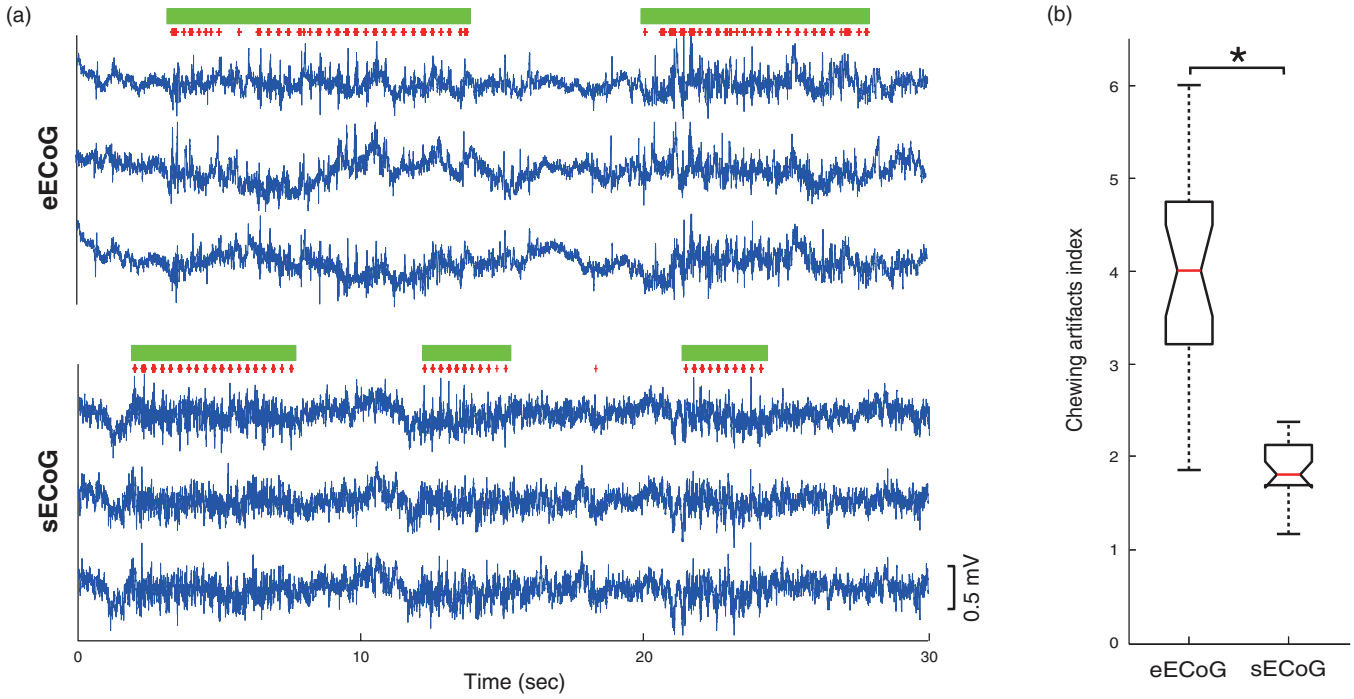

Figure 5. Comparison of signal quality between eECoG signals and sECoG signals. (a) Representative eECoG and sECoG signals from three electrodes. Red asterisks indicate time points with chewing artifacts identified by our algorithm (see section 2 and figure 1(d)). The scale for signal amplitude is shown at the lower right corner. (b) Chewing artifacts index. The medians and lower and upper quartiles are shown in box plots (outliers, including two outliers in the eECoG data and one in the sECoG data, are not shown). There was a significant difference in chewing artifacts indices between eECoG and sECoG signals (asterisk, $p < 0.05$).

correlation between the chewing artifacts index and the prediction accuracy for decoding 3D hand positions. Most artifacts are non-cerebral in origin, including the electromyographic activity produced by muscle contraction. In the eECoG decoding experiments, the eECoG electrodes and the reference electrodes were located closer to the source of the artifacts, making it more likely that artifacts would be detected and lead to incorrect decoding [39–41]. In contrast, the sECoG electrodes and the reference electrodes were implanted underneath the dura, so artifacts might be filtered out or at least weakened by the dura and/or the cerebrospinal fluid (CSF) [12, 13]. In addition, the locations of the reference and ground electrodes were different between eECoG and sECoG (see details in section 2.1), which might also contribute to different artifact levels between eECoG and sECoG. A higher level of artifacts could make the extraction of motor information more difficult, i.e. lower the quality of motor information in recoded signals.

As well as filtering out artifacts in sECoG recordings, the dura and/or the CSF could also filter out detailed motor information in eECoG recordings. This filtering effect would reduce the quantity of motor information available for motor decoding in eECoG experiments. A study in humans showed that the signal power detected in eECoG experiments is ∼20% lower than that detected in sECoG experiments because of signal attenuation caused by the dura [42]. Moreover, a simulation study demonstrated that the amplitude of brain signals could be attenuated by the thickness of CSF [43].

4.2. Durability and stability in eECoG-based decoding

The duration of implantation in this study was 5–6 months, and the experiments were performed during the last two months of this period, where no significant monotonic decrease was found (figure 3(a)). Thus it is expected that the eECoG system could be durable for at least five months, suggesting that the present system has good potential for long-term use.

On the other hand, in cross-day predictions, the eECoG-based model showed similar decoding performance for a shorter period of time (9 days for monkey B, 20 days for monkey C), with gradual deterioration of performance following this period. By contrast, our previous report of sECoG-based decoding showed that the performances of both same-day and cross-day predictions were retained for at least several months [9]. This suggests that the eECoG system is durable but that it is less stable than the sECoG system so that, for practical use, it might require more frequent (once a week) updating of the model than sECoG.

The lower stability of the eECoG-based model might be due to contamination of eECoG signals with noise. The model constructed in each recording session was optimized with informative signals and even unstable artifacts. Therefore, it could be difficult to decode a specific day's dataset using a model that was optimized for another day's dataset when the quality of the signals, represented by the chewing artifacts index, is different from one day to another. Indeed, the distribution of chewing artifacts index from eECoG signals was significantly broader than and different from that from sECoG signals (figure 6(b); $p < 0.05$, $n = 60$ correlation

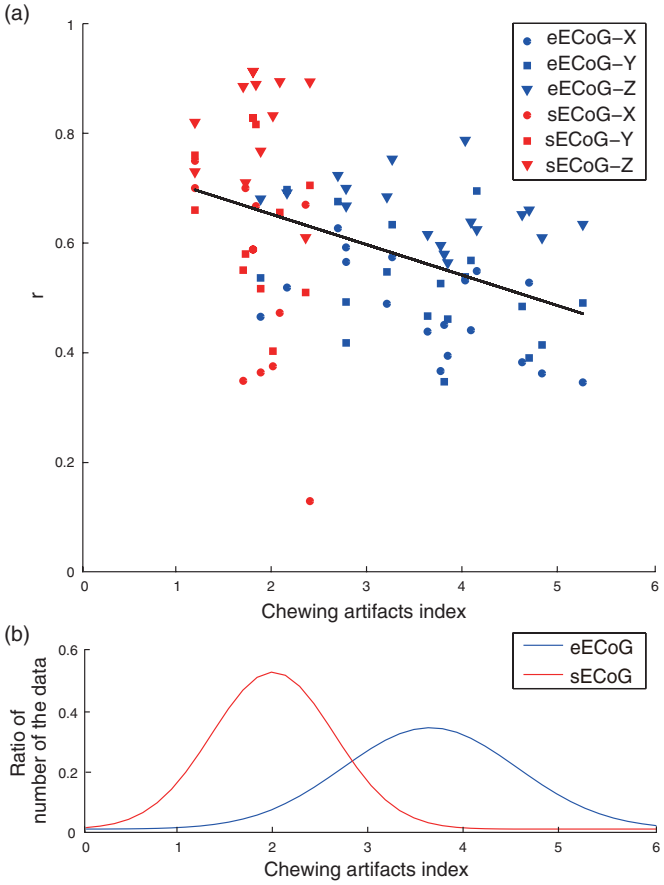

Figure 6. Effects of artifacts on decoding performance. (a) The performance of same-day predictions quantified by the correlation coefficients (r) for X-, Y-, and Z-positions are shown as circles, squares, and triangles, respectively, for eECoG- (symbols in blue) and sECoG-based decoding (symbols in red). A significant monotonic decrease in decoding accuracy was observed with increasing chewing artifacts index ($p < 0.05$, $\varrho = -0.39$, $n = 60$ correlation coefficients for eECoG, and 39 correlation coefficients for sECoG, Spearman rank correlation test), as indicated by the fitted 1-degree polynomial (black line). As in figure 5(b), three outliers are not shown. (b) The distributions of chewing artifacts index for sECoG and eECoG datasets are shown. Red and blue lines represent histograms of points in figure 6(a) for sECoG and eECoG datasets, respectively, fitted by a Gaussian function.

coefficients for eECoG, and 39 for sECoG, F-test). Thus, we suspect that such variation in datasets affected the accuracy of cross-day predictions in eECoG experiments, and this variation underlies the decreased stability of eECoG compared with sECoG. One possible solution that could compensate for the variation in noise is using artifact removal algorithms; this approach could improve the stability as well as the durability of the system (see section 4.4 for details).

The variability of noise and/or signals in eECoG might have decreased the stability of the eECoG-based model. The reason for the instability of noise and/or signals is still unclear. One possible explanation is that a continuous tissue reaction produced granulation and effusion around the electrodes, which might have gradually altered the noise and/or signals in eECoG. In our experience, sECoG causes less granulation than eECoG. The development of a fully implantable wireless recording system could reduce the amounts of infection and granulation tissue by wound closure, and thus improve the decoding stability. Furthermore, when applying decoding to BMI applications, users could adapt to the continuous changes in noise and/or signals, i.e. the same decoder could be used for a longer period of time. This has been demonstrated in SUA studies, where recalibration was needed daily in off-line decoding where no adaptation occurred [14], but was extended to several weeks in BMI applications [44, 45].

4.3. Spatial, spectral and temporal contents in decoding models

Significant differences in decoding models were found between monkeys B and C, especially in terms of their spatial and spectral contributions (figure 4 and also summarized in table 2). Significant spatial contributions of the PMd were found in monkey B, but not in monkey C. Conversely, significant spatial contributions of the PFC, S1 and M1 were found in monkey C, but not in monkey B. Significant spectral contributions were in the range of 40–90 Hz (high-γ band) in monkey B, but were in the range of 10–30 Hz (β band) in monkey C. There are several possible explanations for these differences. In monkey C, a set of nodule-type electrodes was implanted around the motor cortex, including the PMd, and removed several months before the present study (see section 2.1). Tissue growth could occur postoperatively beneath the dura, and this could have reduced the quality of the signals acquired around the area and thus affected the spatial information available for decoding [46–49]. Moreover, the new tissues could act as a low-pass filter, similar to the skull, which shifts the spectrum of useful information available for decoding from the high-γ band to the β band. Furthermore, differences in training level or motor experience could also lead to differences in spatial contributions [50, 51]. The fact that a significant spatial contribution of S1 was found in monkey C suggests that information in sensory afferent signals may have been used for decoding. In the PMd of monkey C, the granulation tissue was generated by the previous surgical procedure. Thus, this area carried fewer brain signals, and the spatial contribution of S1 was relatively increased. In contrast, a significant spatial contribution of S1 could not be found in monkey B because sufficient information for prediction was captured from the PMd.

The decoding models in monkey B, which had not been subjected to any previous operation, demonstrated similar spatial, spectral, and temporal contents compared with the sECoG-based decoding models in our previous study [9] (table 2). The similarities included the following: significant spatial contributions from the PMd; significant spectral contributions from the high-γ band (40–90 Hz); and significant temporal distributions within 500 ms of movement onsets. High-γ band activity in the PMd has been found to be responsible for the control of complex motor outputs.

Despite the significant differences in spatial and spectral contributions between decoding models from monkeys B and C, the prediction accuracies obtained from those two monkeys were comparable. In monkey C, the signals from the PMd and the high-γ band activity might have been blocked or filtered out

Table 2. Comparison of spatio-spectro-temporal contributions.

		Spatial contribution			Spectral contribution (Hz)			
Type of electrodes	Monkeys	X	Y	Z	X	Y	Z	Temporal contribution (ms)
eECoG	B	PMd	PMd	PMd	40–70	50–90	40–90	−100 to −500
	C	PFC S1	PFC S1 M1	PFC S1 M1	10–30	10–30	10–30	−100 to −500
sECoG	A	PMd	PMd M1	PMv M1	40–90	40–90	40–90	−100 to −500
	K	PMd M1	PMd M1	PMd M1	40–90	40–90	40–90	−100 to −500

Abbreviations: PMd, dorsal premotor cortex; PFC, prefrontal cortex; S1, primary somatosensory cortex; M1, primary motor cortex; PMv, ventral premotor cortex.

by new tissues that formed postoperatively. The comparable accuracy in monkey C to that in monkey B could be achieved by incorporating the spatial and spectral integration of activity across multiple cortical areas to compensate for the loss of information from the PMd and high-γ band activity. In monkey B, the contributions of the decoding model constructed without using brain information from the PMd and high-γ band activity might have been similar to those in monkey C. On the basis of the differences in spatial and spectral contributions between monkeys B and C, it might be better to record brain activity not only from the area of the brain significantly related to the motor intention, but also the surrounding area, using a broad frequency bandwidth to compensate for the low fidelity in other brain areas. From this reason, the proposed model has been shown to be robust to the differences in spatial and spectral contributions.

4.4. Improving performance for BMI

The prediction accuracy of eECoG-based decoding was on average 47% higher than that of EEG-based decoding during a 3D center-out reaching task [8], although it was slightly lower than that of sECoG-based decoding [9]. We propose three approaches that can be used to improve the performance of eECoG-based decoding for real-time BMI applications.

First, we found that the chewing artifacts index in eECoG signals was significantly higher than that in sECoG signals (figure 5(b)). In addition, the artifacts decreased the accuracy and stability of eECoG-based predictions (figure 6(a) and 3(b)). These findings indicate that eECoG is more sensitive to contamination from artifacts, such as electrical muscle activity (e.g. blink, ocular movement and chewing) than sECoG. One way to decrease the effects of these artifacts is using real-time artifact removal algorithms, which have been developed in EEG-based decoding studies and shown to improve performance [52, 53].

Second, in general, BMI uses brain signals recorded from a single hemisphere contralateral to the working limb because the information representing motor output is associated with the motor cortex in the contralateral cerebral hemisphere. However, several studies have recently demonstrated that the motor cortex is involved in not only contralateral body movements, but also ipsilateral ones [11, 54–58]. Therefore, the decoding performance could be improved by using information from the ipsilateral cerebral hemisphere as well as the contralateral hemisphere if we could overcome the risk of complications due to implanting electrodes in both hemispheres.

Third, if we apply eECoG-based decoding to real-time BMI applications, visual feedback would compensate for the prediction error and improve device control performance over time [4, 5, 10, 59, 60]. Indeed, a 2D computer cursor was accurately controlled following a week of on-line visual feedback training in eECoG-based BMI experiments [33].

If we can successfully employ these modifications, the performance of eECoG decoding will be significantly increased and the advantages of eECoG will be enhanced.

5. Conclusion

We found that eECoG signals carry sufficient information for asynchronous decoding of continuous 3D hand trajectories. As one of the safest available invasive recording methods, eECoG provides an adequate level of decoding accuracy, durability and stability. With ease of replacement and upgrades, eECoG could deliver further practicality, versatility and clinical friendliness for BMI applications.

Acknowledgments

Partial support was provided through the Strategic Research Program for Brain Science by MEXT Japan. We thank Naomi Hasegawa and Tomonori Notoya for handling and caring for the animals, as well as Kazuhito Takenaka for helping with the data analysis. We gratefully acknowledge the valuable comments with Yoichi Katayama, Takamitsu Yamamoto, and Chikashi Fukaya.

References

[1] Wolpaw J R, Birbaumer N, McFarland D J, Pfurtscheller G and Vaughan T M 2002 Brain-computer interfaces for communication and control *Clin. Neurophysiol.* **113** 767–91

[2] Birbaumer N, Ghanayim N, Hinterberger T, Iversen I, Kotchoubey B, Kubler A, Prelmouter J, Taub E and Flor H 1999 A spelling device for the paralysed *Nature* **398** 297–8

[3] Wolpaw J R and McFarland D J 2004 Control of a two-dimensional movement signal by a noninvasive brain-computer interface in humans *Proc. Natl Acad. Sci. USA* **101** 17849–54

[4] Leuthardt E C, Schalk G, Wolpaw J R, Ojemann J G and Moran D W 2004 A brain-computer interface using electrocorticographic signals in humans *J. Neural Eng.* **1** 63–71

[5] Schalk G, Miller K J, Anderson N R, Wilson J A, Smyth M D, Ojemann J G, Moran D W, Wolpaw J R and Leuthardt E C 2008 Two-dimensional movement control using electrocorticographic signals in humans *J. Neural Eng.* **5** 75–84

[6] Yanagisawa T, Hirata M, Saitoh Y, Goto T, Kishima H, Fukuma R, Yokoi H, Kamitani Y and Yoshimine T 2011 Real-time control of a prosthetic hand using human electrocorticography signals *J. Neurosurg.* **114** 1715–22

[7] Ball T, Kern M, Mutschler I, Aertsen A and Schulze-Bonhage A 2009 Signal quality of simultaneously recorded invasive and non-invasive EEG *Neuroimage* **46** 708–16

[8] Bradberry T J, Gentili R J and Contreras-Vidal J L 2010 Reconstructing three-dimensional hand movements from noninvasive electroencephalographic signals *J. Neurosci.* **30** 3432–7

[9] Chao Z C, Nagasaka Y and Fujii N 2010 Long-term asynchronous decoding of arm motion using electrocorticographic signals in monkeys *Front. Neuroeng.* **3** 3

[10] Leuthardt E C, Schalk G, Roland J, Rouse A and Moran D W 2009 Evolution of brain-computer interfaces: going beyond classic motor physiology *Neurosurg. Focus* **27** E4

[11] Lebedev M A, O'Doherty J E and Nicolelis M A 2008 Decoding of temporal intervals from cortical ensemble activity *J. Neurophysiol.* **99** 166–86

[12] Carmena J M, Lebedev M A, Crist R E, O'Doherty J E, Santucci D M, Dimitrov D F, Patil P G, Henriquez C S and Nicolelis M A 2003 Learning to control a brain-machine interface for reaching and grasping by primates *PLoS Biol.* **1** E42

[13] Wessberg J, Stambaugh C R, Kralik J D, Beck P D, Laubach M, Chapin J K, Kim J, Biggs S J, Srinivasan M A and Nicolelis M A 2000 Real-time prediction of hand trajectory by ensembles of cortical neurons in primates *Nature* **408** 361–5

[14] Chestek C A, Batista A P, Santhanam G, Yu B M, Afshar A, Cunningham J P, Gilja V, Ryu S I, Churchland M M and Shenoy K V 2007 Single-neuron stability during repeated reaching in macaque premotor cortex *J. Neurosci.* **27** 10742–50

[15] Leuthardt E C, Schalk G, Moran D and Ojemann J G 2006 The emerging world of motor neuroprosthetics: a neurosurgical perspective *Neurosurgery* **59** 1–14

[16] Fountas K N and Smith J R 2007 Subdural electrode-associated complications: a 20-year experience *Stereotact. Funct. Neurosurg.* **85** 264–72

[17] Van Gompel J J, Worrell G A, Bell M L, Patrick T A, Cascino G D, Raffel C, Marsh W R and Meyer F B 2008 Intracranial electroencephalography with subdural grid electrodes: techniques, complications, and outcomes *Neurosurgery* **63** 498–505

[18] Wong C H, Birkett J, Byth K, Dexter M, Somerville E, Gill D, Chaseling R, Fearnside M and Bleasel A 2009 Risk factors for complications during intracranial electrode recording in presurgical evaluation of drug resistant partial epilepsy *Acta. Neurochir. (Wien)* **151** 37–50

[19] Hamer H M *et al* 2002 Complications of invasive video-EEG monitoring with subdural grid electrodes *Neurology* **58** 97–103

[20] Morrell M J 2011 Responsive cortical stimulation for the treatment of medically intractable partial epilepsy *Neurology* **77** 1295–304

[21] Tsubokawa T, Katayama Y, Yamamoto T, Hirayama T and Koyama S 1993 Chronic motor cortex stimulation in patients with thalamic pain *J. Neurosurg.* **78** 393–401

[22] Katayama Y, Fukaya C and Yamamoto T 1998 Poststroke pain control by chronic motor cortex stimulation: neurological characteristics predicting a favorable response *J. Neurosurg.* **89** 585–91

[23] Levy R, Ruland S, Weinand M, Lowry D, Dafer R and Bakay R 2008 Cortical stimulation for the rehabilitation of patients with hemiparetic stroke: a multicenter feasibility study of safety and efficacy *J. Neurosurg.* **108** 707–14

[24] Nguyen J P *et al* 1999 Chronic motor cortex stimulation in the treatment of central and neuropathic pain. Correlations between clinical, electrophysiological and anatomical data *Pain* **82** 245–51

[25] Nguyen J P, Velasco F, Brugieres P, Velasco M, Keravel Y, Boleaga B, Brito F and Lefaucheur J P 2008 Treatment of chronic neuropathic pain by motor cortex stimulation: results of a bicentric controlled crossover trial *Brain Stimul.* **1** 89–96

[26] Molina-Luna K, Buitrago M M, Hertler B, Schubring M, Haiss F, Nisch W, Schulz J B and Luft A R 2007 Cortical stimulation mapping using epidurally implanted thin-film microelectrode arrays *J. Neurosci. Methods* **161** 118–25

[27] Procter L D, Davenport D L, Bernard A C and Zwischenberger J B 2010 General surgical operative duration is associated with increased risk-adjusted infectious complication rates and length of hospital stay *J. Am. Coll. Surg.* **210** 60–5

[28] Uejima T, Kita K, Fujii T, Kato R, Takita M and Yokoi H 2009 Motion classification using epidural electrodes for low-invasive brain-machine interface *Conf. Proc. IEEE Eng. Med. Biol. Soc., 2009* pp 6469–72

[29] Slutzky M W, Jordan L R, Lindberg E W, Lindsay K E and Miller L E 2011 Decoding the rat forelimb movement direction from epidural and intracortical field potentials *J Neural Eng.* **8** 036013

[30] Slutzky M W, Lindberg E W, Jordan L R and Miller L E 2010 Decoding motor outputs with epidural and intracortical inputs: performance similarities and differences *2010 Neuroscience Meeting Planner (San Diego, CA, Society for Neuroscience)* 383.16/AAA6

[31] Gomez-Rodriguez M, Grosse-Wentrup M, Peters J, Naros G, Hill J, Scholkopf B and Gharabaghi A 2010 Epidural ECoG online decoding of arm movement intention in hemiparesis *Conf. Proc. ICPR Workshop on Brain Decoding* 2010 pp 1–4

[32] Rouse A G, Heldman D A and Moran D W 2007 Neural adaptation of epidural electrocorticographic (EECoG) signals during closed-loop brain computer interface (BCI) control *2007 Neuroscience Meeting Planner (San Diego, CA, Society for Neuroscience)* 192.7/UU22

[33] Rouse A G and Moran D W 2009 Neural adaptation of epidural electrocorticographic (EECoG) signals during closed-loop brain computer interface (BCI) tasks *Conf. Proc. IEEE Eng. Med. Biol. Soc. 2009* pp 5514–7

[34] Rouse A G, Williams J J, Wheeler J J and Moran D W 2010 The effect of electrode distance and neural plasticity on an epidural electrocorticographic (EECoG) closed-loop brain–computer interface (BCI) *2010 Neuroscience Meeting Planner (San Diego, CA, Society for Neuroscience)* 85.14/AAA22

[35] Williams J J, Rouse A G, Wheeler J J, Williams J C and Moran D W 2010 Evaluation of impedance, signal quality, and neural plasticity characteristics in a chronic micro-ECoG device *2010 Neuroscience Meeting Planner (San Diego, CA, Society for Neuroscience)* 85.13/AAA21

[36] Kennedy P, Andreasen D, Ehirim P, King B, Kirby T, Mao H and Moore M 2004 Using human extra-cortical local field potentials to control a switch *J. Neural Eng.* **1** 72–7

[37] Leuthardt E C, Miller K J, Schalk G, Rao R P N and Ojemann J G 2006 Electrocorticography-based brain computer interface-the Seattle experience *IEEE Trans. Neural Syst. Rehabil. Eng.* **14** 194–8

[38] Nagasaka Y, Shimoda K and Fujii N 2011 Multidimensional recording (MDR) and data sharing: an ecological open research and educational platform for neuroscience *PLoS One* **6** e22561

[39] McFarland D J, Sarnacki W A, Vaughan T M and Wolpaw J R 2005 Brain-computer interface (BCI) operation: signal and noise during early training sessions *Clin. Neurophysiol.* **116** 56–62

[40] Vaughan T M *et al* 2003 Brain-computer interface technology: a review of the second international meeting *IEEE Trans. Neural Syst. Rehabil. Eng.* **11** 94–109

[41] Goncharova II, McFarland D J, Vaughan T M and Wolpaw J R 2003 EMG contamination of EEG: spectral and topographical characteristics *Clin. Neurophysiol.* **114** 1580–93

[42] Torres Valderrama A, Oostenveld R, Vansteensel M J, Huiskamp G M and Ramsey N F 2010 Gain of the human dura *in vivo* and its effects on invasive brain signal feature detection *J. Neurosci. Methods* **187** 270–9

[43] Slutzky M W, Jordan L R, Krieg T, Chen M, Mogul D J and Miller L E 2010 Optimal spacing of surface electrode arrays for brain-machine interface applications *J. Neural Eng.* **7** 26004

[44] Ganguly K and Carmena J M 2009 Emergence of a stable cortical map for neuroprosthetic control *PLoS Biol.* **7** e1000153

[45] Pohlmeyer E A, Oby E R, Perrault E J, Solla S A, Kilgore K L, Kirsch R F and Miller L E 2009 Toward the restoration of hand use to paralyzed monkey: brain-controlled functional electrical stimulation of forearm muscles *PLoS One* **4** e5924

[46] Yuen T G, Agnew W F and Bullara L A 1987 Tissue response to potential neuroprosthetic materials implanted subdurally *Biomaterials* **8** 138–41

[47] Biran R, Martin D C and Tresco P A 2005 Neuronal cell loss accompanies the brain tissue response to chronically implanted silicon microelectrode arrays *Exp. Neurol.* **195** 115–26

[48] Polikov V S, Tresco P A and Reichert W M 2005 Response of brain tissue to chronically implanted neural electrodes *J. Neurosci. Methods* **148** 1–18

[49] Williams J C, Hippensteel J A, Dilgen J, Shain W and Kipke D R 2007 Complex impedance spectroscopy for monitoring tissue responses to inserted neural implants *J. Neural Eng.* **4** 410–23

[50] Mitz A R, Godschalk M and Wise S P 1991 Learning-dependent neuronal activity in the premotor cortex: activity during the acquisition of conditional motor associations *J. Neurosci.* **11** 1855–72

[51] Laubach M, Wessberg J and Nicolelis M A 2000 Cortical ensemble activity increasingly predicts behaviour outcomes during learning of a motor task *Nature* **405** 567–71

[52] Croft R J and Barry R J 2000 Removal of ocular artifact from the EEG: a review *Neurophysiol. Clin.* **30** 5–19

[53] Gao J F, Yang Y, Lin P, Wang P and Zheng C X 2010 Automatic removal of eye-movement and blink artifacts from EEG signals *Brain Topogr.* **23** 105–14

[54] Rao S M *et al* 1993 Functional magnetic resonance imaging of complex human movements *Neurology* **43** 2311–8

[55] Boecker H, Kleinschmidt A, Requardt M, Hanicke W, Merboldt K D and Frahm J 1994 Functional cooperativity of human cortical motor areas during self-paced simple finger movements. A high-resolution MRI study *Brain* **117** 1231–9

[56] Li A, Yetkin F Z, Cox R and Haughton V M 1996 Ipsilateral hemisphere activation during motor and sensory tasks *AJNR Am. J. Neuroradiol.* **17** 651–5

[57] Baraldi P, Porro C A, Serafini M, Pagnoni G, Murari C, Corazza R and Nichelli P 1999 Bilateral representation of sequential finger movements in human cortical areas *Neurosci. Lett.* **269** 95–8

[58] Ganguly K *et al* 2009 Cortical representation of ipsilateral arm movements in monkey and man *J. Neurosci.* **29** 12948–56

[59] Taylor D M, Tillery S I and Schwartz A B 2002 Direct cortical control of 3D neuroprosthetic devices *Science* **296** 1829–32

[60] Suminski A J, Tkach D C, Fagg A H and Hatsopoulos N G 2010 Incorporating feedback from multiple sensory modalities enhances brain-machine interface control *J. Neurosci.* **30** 16777–87